AIAA 2005-5050

36th AIAA Plasmadynamics and Laser Conference
June 6- 9, 2005, Toronto, Ontario, Canada

AIAA 2005-5050

Numerical Simulation of Secondary Flow in a Weakly Ionized Supersonic Flow with Applied Electromagnetic Field

Pradeep S. Rawat*, Xiaolin Zhong† and Varun Singh‡
University of California, Los Angeles, CA, 90095

and

Sivaram Gogineni§
Innovative Scientific Solutions, Inc., Dayton, Ohio

Abstract

This paper investigates, by numerical simulation of Navier Stokes equations, Magnetohydrodynamic (MHD) effects of an imposed electromagnetic field on secondary flow in a plasma wind tunnel with a weakly ionized supersonic flow in the range of Mach number 2.6 to 3.0. The imposed magnetic field is generated by a magnet flush-mounted in the tunnel side wall. Flow is pre-ionized by an R-F discharge and DC electric field is generated in the flow by electrodes flush-mounted in the top and bottom walls, perpendicular both to the flow velocity and the magnetic field. The electrical conductivity of the flow varies between 0.1 and 0.5 mho/m. The magnetic Reynolds number of the flow is small so induced magnetic field is neglected. The governing equations of the MHD flow, which are the Navier-Stokes equations with the applied electromagnetic force terms, are computed by a third-order upwind numerical scheme. A series of cases with different imposed magnetic fields, electric fields and electrical conductivities, for two different stagnation pressures at the nozzle entrance, were investigated. A strong secondary flow was observed in the cold flow, i.e. flow with magnetic field and electric field switched off. However when a strong electric field is applied at constant electrical conductivity, the Mach number in the inviscid core is seen to drop. Also, the boundary layer thickness increases. More importantly, the strong cross flow is reduced downstream of the zone of electric field imposition. The negative magnetic field, acting in conjunction with the strong electric field further retards the flow and generates stronger secondary flow. To account for the scenario when time lag is large between application of electromagnetic field and Joule heating of flow, calculations were carried out by neglecting Joule heating terms in energy equation. Actual solutions are expected to be in between those obtained with and without considering Joule heating effects. In absence of Joule heating, constant acceleration (retardation) of flow was observed with accelerating (retarding) electromagnetic field although the changes in flow properties were minor as compared to the Joule heated flow with same electromagnetic fields. Under the assumption of no Joule heating, accelerating magnetic fields reduce the secondary flow while retarding flow makes the secondary flow stronger. Flow with a lower Reynolds number is expected to be more stable because of viscous effects. On the contrary, secondary flow near side wall is observed to be stronger for cold flows of lower Reynolds number. Also, Lower Reynolds number flow is observed to be affected more strongly by applied electromagnetic forces. In general, an accelerating magnetic field applied with electric field was observed to produce much lower secondary flow than the retarding magnetic field in same situation for almost all of the cases considered in the study.

Nomenclature

B	= magnetic field vector	B_x, B_y, B_z	= Cartesian magnetic field components
c	= local speed of sound	C_v	= constant volume specific heat
e	= total energy of fluid	**E**	= electric field vector
J	= Jacobian of grid transformation	**J**	= conduction current density
k	= thermal conductivity	**K**	= surface electric current density

*Graduate Student, Mechanical and Aerospace Engineering Department. Pradeep@seas.ucla.edu
†Professor, Mechanical and Aerospace Engineering Department, Associate Fellow, AIAA.
‡Graduate Student, Mechanical and Aerospace Engineering Department. Student Member, AIAA.
§Senior Engineer, Innovative Scientific Solutions Inc., Associate Fellow, AIAA

M	= Mach number	p	= pressure
P	= Prandtl number	$\mathbf{q}$	= heat flux vector
t	= time	T	= temperature
T_r	= reference temperature	T_∞	= sonic temperature
T_o	= stagnation temperature	u,v,w	= Cartesian velocity components
x,y,z	= Cartesian coordinates	ε_e	= dielectric constant in free space
γ	= ratio of specific heats	μ	= dynamic viscosity
μ_e	= magnetic permeability in free space	ρ	= density of fluid
ρ_e	= local electric charge density	σ	= electrical conductivity of fluid
$\bar{\bar{\tau}}$	= viscous stress tensor		

1 Introduction

Sustained high speed flights offer potentially revolutionary improvements in space access. Factors limiting the performance of a supersonic vehicle include aerodynamic drag and heating rates exerted on the vehicles by surrounding flow fields. Recent research has indicated that supersonic flow fields may be modified significantly by magnetic Lorentz forces through the creation and manipulation of plasma near vehicles [1]. In supersonic flows, the gas becomes weakly ionized either by viscous heating or by artificially generating plasma in the flow. If there is an imposed electromagnetic field in the flow, the flow properties can be changed substantially by the interaction of the electrically conducting gas and the electromagnetic field. Such interaction forms the basic idea of electromagnetic modification of supersonic flow. Secondary flow expedites the process of transition to turbulence in the flow and many researchers have shown that supersonic flow can be altered significantly by Lorentz force [2-13] hence current study aims to investigate control of secondary flow in supersonic flow using electromagnetic forces.

In this paper, a supersonic flow in a three-dimensional expanding test section, with parallel sidewalls, is studied, using numerical simulation, under an externally imposed electromagnetic field. Simulations mirror the conditions of experiments which were conducted in supersonic nonequilibrium plasma/MHD wind tunnel facility at the Nonequilibrium Thermodynamics Laboratories [14-17]. Stable and diffuse supersonic flow of nonequilibrium plasma is generated for this Mach 3 tunnel. Ionization in the test section is produced by a transverse RF discharge sustained between two electrode blocks 3 cm long which are flush mounted in the side test section walls. Each electrode block, manufactured of high-temperature machinable mica ceramic, incorporates three copper strip electrodes 35 mm long and 5 mm wide. An aerodynamically contoured supersonic nozzle made of transparent acrylic plastic is connected to a 2 cm x 4 cm rectangular cross section test section 12 cm long with an angle step diffuser. The nozzle / test section / diffuser assembly is equipped by pressure taps measuring plenum pressure as well as static pressure at the beginning and at the end of the test section. The imposed magnetic field is produced by a permanent magnet, 5 cm in length and as wide as the side wall, starting 10 cm downstream from the entrance of the tunnel flush mounted in the nozzle side wall. The transverse DC electrical current is spatially superimposed on the magnetic field using two copper electrodes flush mounted in the top and bottom nozzle walls, perpendicular to the magnetic field and the flow direction. Optical access to the flow is provided using two 1”x1/2” glass windows in the top and bottom walls of the M=3 test section. The windows are centered in the flow and their width is chosen so as to provide optical access to both side wall boundary layers.

Singh et al [18], investigated the effect of imposed electromagnetic field on a weakly ionized supersonic boundary layer with Mach number in the range of 2.7 to 3.0, for a two dimensional approximation of the current geometry. Electric and magnetic fields were varied and it was found that the temperature at the centerline and boundary layer thickness increased with increasing electric field strength. The magnetic field was found to have a mitigating effect on joule heating when a combination of an electromagnetic field was imposed. However, the two dimensional calculations ignore effect of sidewalls so they are insufficient to capture thick sidewall boundary layer as observed in experiments [15, 16]. Hence a three dimensional study was necessary for more realistic simulations of the flow. Three dimensional simulation show a strong secondary flow near center of sidewall which was in accordance with the experimental observations. In this paper, we focus on estimating effects of electromagnetic fields on this secondary flow.

We have simulated an array of scenario with a variation in the magnetic field strength, electric field strength and electrical conductivity for two different stagnation pressures of one-third atmosphere and one-fifth atmosphere. The imposed magnetic field is taken as spatially and temporally uniform in a direction perpendicular to the flow vector in the spanwise direction for simplicity. Similarly, the electric field is spatially and temporally uniform in a plane perpendicular to the flow vector and the magnetic field vector. Electric conductivity is also assumed to be spatially

uniform. The governing equations for the MHD flow are formulated from the Navier-Stokes and the Maxwell equations, and are spatially discretized by a third-order numerical scheme. In an attempt to solve the coupled MHD equations, difficulties were encountered due to the constraint of the size of time step posed by the magnetic diffusivity of the magnetic induction equation. To resolve the "stiffness" problem, we solve the approximate MHD equations without the induction equation by neglecting the induced magnetic field and assuming that the imposed magnetic field is constant. This is actually a fair assumption considering that the magnetic Reynolds number is of the order of 10^{-3}. We have also conducted simulation of effects of electromagnetic fields on the flow by neglecting Joule heating terms in the governing energy equation so as to account for the case when time lag between application of electromagnetic field and heating of the flow is significantly large. Actual flows are expected to be between the solutions obtained by simulating with and without considering Joule heating effects.

2 Governing Equations

The governing equations of MHD of compressible flow are the Maxwell equations coupled with the Navier-Stokes equations through the momentum and energy equations. The current density **J** in MHD is given by the generalized Ohm's law as follows,

$$\mathbf{J} = \sigma(\mathbf{E} + \mathbf{u} \times \mathbf{B}) \tag{1}$$

where E is the electric field vector and σ is the electrical conductivity. This equation relates the current density with the electric field and the induced electric field generated by crossing the magnetic field lines with the velocity vector. This form of the electric current equation neglects the Hall current for simplicity. In this paper, in order to solve the MHD equations more efficiently, we only consider the cases where the small magnetic Reynolds number assumption applies. The magnetic Reynolds number defined as ULσμe is in the order of 10-3 for all cases presented in this paper, where σ is the electrical conductivity of fluid and μe is the magnetic permeability in free space. Since it is much less than unity, we assume that the induced magnetic field is negligible and the imposed magnetic field is constant through all the computations.

The set of MHD equations with the assumption of negligible induced magnetic field are written as follows:

$$\frac{\partial \rho}{\partial t} + \nabla.(\rho \mathbf{u}) = 0 \tag{2}$$

$$\rho\left(\frac{\partial \mathbf{u}}{\partial t} + \mathbf{u} \cdot \nabla \mathbf{u}\right) = -\nabla p + \nabla \cdot \overline{\overline{\tau}} + \sigma(\mathbf{E} \times \mathbf{B}) + \sigma(\mathbf{u} \times \mathbf{B}) \times \mathbf{B} \tag{3}$$

$$\frac{\partial e}{\partial t} + \nabla \cdot (e\mathbf{u}) = -\nabla \cdot (p\mathbf{u}) + \nabla \cdot (\mathbf{u} \cdot \overline{\overline{\tau}}) - \nabla \cdot \mathbf{q} + \mathbf{E} \cdot \mathbf{J} \tag{4}$$

where $e = \frac{p}{(\gamma - 1)} + \frac{1}{2}\rho U^2$, is the internal energy plus the kinetic energy of the fluid. The viscous stress and the heat flux are given by the usual constitutive equations in Newtonian fluid as follows

$$\tau_{ij} = \mu\left(\frac{\partial u_i}{\partial x_j} + \frac{\partial u_j}{\partial x_i}\right) - \frac{2}{3}\mu\frac{\partial u_k}{\partial x_k}\delta_{ij} \quad \text{and} \quad q_i = -k\frac{\partial T}{\partial x_i} \text{ where } \mu = \mu_r\left(\frac{T}{T_r}\right)^{\frac{3}{2}}\frac{T_r + T_s}{T + T_s} \tag{5}$$

Viscosity coefficient, μ is determined by the Sutherland law. Where T_r = 288K, T_s = 110K and μ_r = 0.17894 × 10^{-4} kg/m/s for air. The thermal conductivity k is computed from the Prandtl number, which is assumed constant and it takes the value of 0.72 in this paper.

The imposed magnetic field is taken as spatially and temporally uniform in a direction perpendicular to the flow vector in the spanwise direction for simplicity. The electric field is spatially and temporally uniform in a plane perpendicular to the flow vector and the magnetic field vector for simplicity.

3 Numerical Method

There have been several recent works on developing upwind schemes for MHD equations with shock capturing capability [19, 20]. Most of these methods are second order accurate TVD schemes. But these schemes were not used in this paper since future scope of the current work includes stability analysis demanding more accurate and robust calculations. We use a third-order finite difference scheme that we have developed and validated for solving the full Navier-Stokes equation for spatial discretization of the MHD equations [21]. The numerical method used in this study is briefly summarized in this section. More details on the method and its validations can be found in [21].

In numerical simulation, the MHD equations (2) to (4) are written in the following conservative form,

$$\frac{\partial U}{\partial t}+\frac{\partial E}{\partial x}+\frac{\partial F}{\partial y}+\frac{\partial G}{\partial z}+\frac{\partial E_v}{\partial x}+\frac{\partial F_v}{\partial y}+\frac{\partial G_v}{\partial z}=M \tag{6}$$

U consists of conservative variables while E, F, G are the inviscid flux terms, and E_v, F_v, G_v are the viscous terms, and M is the MHD source term. They are written as follows

$$U=\{\rho,\rho u,\rho v,\rho w,e\},\ E=\begin{Bmatrix}\rho u\\ \rho u^2+p\\ \rho uv\\ \rho uw\\ (e+p)u\end{Bmatrix},\ F=\begin{Bmatrix}\rho v\\ \rho vu\\ \rho v^2+p\\ \rho vw\\ (e+p)v\end{Bmatrix},\ G=\begin{Bmatrix}\rho w\\ \rho wu\\ \rho wv\\ \rho w^2+p\\ (e+p)w\end{Bmatrix}$$

$$E_v=\begin{Bmatrix}0\\ \tau_{xx}\\ \tau_{yx}\\ \tau_{zx}\\ u\tau_{xx}+v\tau_{yx}+w\tau_{zx}-q_x\end{Bmatrix},\ F_v=\begin{Bmatrix}0\\ \tau_{xy}\\ \tau_{yy}\\ \tau_{zy}\\ u\tau_{xy}+v\tau_{yy}+w\tau_{zy}-q_y\end{Bmatrix},\ G_v=\begin{Bmatrix}0\\ \tau_{xz}\\ \tau_{yz}\\ \tau_{zz}\\ u\tau_{xz}+v\tau_{yz}+w\tau_{zz}-q_z\end{Bmatrix}$$

and

$$M=\sigma\begin{Bmatrix}0\\ -u\left(B_y^2+B_z^2\right)+v\left(B_xB_y\right)+w\left(B_xB_z\right)+E_yB_z-E_zB_y\\ u\left(B_xB_y\right)-v\left(B_x^2+B_z^2\right)+w\left(B_yB_z\right)+E_zB_x-E_xB_z\\ u\left(B_xB_z\right)+v\left(B_yB_z\right)-w\left(B_x^2+B_y^2\right)+E_xB_y-E_yB_x\\ E_x^2+E_y^2+E_z^2+v\left(E_xB_z-E_zB_x\right)+w\left(E_yB_x-E_xB_y\right)+u\left(E_zB_y-E_yB_z\right)\end{Bmatrix} \tag{7}$$

In the conservative Eq. (6), the inviscid fluxes and the viscous fluxes have the same forms as those of the Navier-Stokes equations. The new term, M, represents the contribution of the Lorentz force.

Before discretizing the governing equations by a finite difference method, Eq. (6) in the physical domain is transformed to the body-fitted computational domain by the following transformation relations,

$$\begin{cases} \xi = \xi(x,y,z) \\ \eta = \eta(x,y,z) \\ \varsigma = \varsigma(x,y,z) \\ \tau = t \end{cases} \Leftrightarrow \begin{cases} x = x(\xi,\eta,\varsigma,\tau) \\ y = y(\xi,\eta,\varsigma,\tau) \\ z = z(\xi,\eta,\varsigma,\tau) \\ t = \tau \end{cases} \tag{8}$$

The transformed governing equation in the computational domain is expressed as follows

$$\frac{1}{J}\frac{\partial U}{\partial \tau} + \frac{\partial E'}{\partial \xi} + \frac{\partial F'}{\partial \eta} + \frac{\partial G'}{\partial \varsigma} + \frac{\partial E'_v}{\partial \xi} + \frac{\partial F'_v}{\partial \eta} + \frac{\partial G'_v}{\partial \varsigma} + U\frac{\partial\left(\frac{1}{J}\right)}{\partial \tau} = M \tag{9}$$

A third-order explicit finite difference scheme is used for spatial discretization of the governing Eq.(9), the inviscid flux terms are discretized by the upwind scheme, and the viscous flux terms are discretized by the central scheme. For the inviscid flux vectors, the flux Jacobians contain both positive and negative eigenvalues, a simple local Lax-Friedrichs scheme is used to split vectors into negative and positive wave fields. For example, the flux term F′ in Eq. (9) can be split into two terms of pure positive and negative eigenvalues as follows

$$F' = F'_+ + F'_- \qquad \text{Where } F'_+ = \frac{1}{2}\left(F' + \lambda U\right) \text{and } F'_- = \frac{1}{2}\left(F' - \lambda U\right) \tag{10}$$

and λ is chosen to be larger than the local maximum eigenvalue of F′.

$$\lambda = \frac{|\nabla\eta|}{J}\left(\sqrt{(\varepsilon c)^2 + u'^2} + c\right) \qquad \text{where} \qquad u' = \frac{\eta_x u + \eta_y v + \eta_z w + \eta_t}{|\nabla\eta|} \tag{11}$$

The parameter ε is a small positive constant added to adjust the smoothness of the splitting. The fluxes F'_+ and F'_- contain only positive and negative eigenvalues respectively. Therefore, in the spatial discretization of Eq. (9), the derivative of the flux F is split into two terms

$$\frac{\partial F'}{\partial \eta} = \frac{\partial F'_+}{\partial \eta} + \frac{\partial F'_-}{\partial \eta} \tag{12}$$

The first term on the right hand side is the discretized by the upwind scheme and the second term by the downwind scheme.

4 Boundary Conditions

Flow in the tunnel is symmetric about horizontal and vertical planes at the centerline of tunnel so only a quarter of actual domain is computed. The computational domain is presented in Fig. 1(a). Boundary conditions for this domain are presented below.

4.1 Upper boundary

Upper boundary serves as a horizontal plane of symmetry for all flow variables. The imposed electromagnetic field has no effect at the plane of symmetry.

4.2 Lower boundary

The wall of the tunnel itself is the lower computational boundary, it is assumed to be adiabatic so at the lower boundary $\frac{\partial T}{\partial y} = 0$. The velocity components *u* and *w* are zero following the non-slip wall condition and *v* is zero

according to the solid-wall condition. For the magnetic field lines across the lower boundary, the normal component of the magnetic field across the wall is continuous. The tunnel wall is assumed non-magnetic such that the tangential component across the boundary is given by

$$\hat{\mathbf{n}} \times (\mathbf{B}_2 - \mathbf{B}_1) = \mu_e \mathbf{K} \tag{13}$$

Where $\hat{\mathbf{n}}$ is the surface normal vector and $\mathbf{K}$ is the surface current density. We assume that the wall is electrically insulated, therefore the surface current density is zero and the tangential component of the magnetic field is continuous across the wall.

4.3 Left boundary

The far side boundary serves as a vertical plane of symmetry for all flow variables in the spanwise direction. Only one half of the physical domain in the spanwise direction is computed. The electromagnetic field has no effect at the plane of symmetry.

4.4 Right boundary

The near side boundary of the computational domain is the wall of the tunnel. It is assumed to be adiabatic, i.e. $\frac{\partial T}{\partial z} = 0$ is enforced at the boundary. The velocity components *u* and *v* are zero following the non-slip condition and *w* is zero according to the solid-wall condition. For the magnetic field lines across the near side boundary, the normal component of the magnetic field across the wall is continuous. The tunnel wall is assumed non-magnetic such that the tangential component across the boundary is given by Eq.13. We assume that the wall is electrically insulated, therefore the surface current density is zero and the tangential component of the magnetic field is continuous across the wall.

4.5 Inlet and exit conditions

Flow entering the tunnel should have a developed boundary for realistic calculations. For this purpose, a separate simulation of an inlet channel is performed prior to simulating nozzle flow. This inlet channel have same rectangular cross section everywhere as that of the nozzle throat. Simulations are performed for a uniform flow entering the inlet channel at a Mach number slightly greater than the sonic flow. Along the inlet channel a location is chosen where sonic flow is obtained in inviscid core with a developed boundary. Flow properties at this location are used as fixed inlet condition for the actual simulation of nozzle. At exit of the nozzle section, the flow variables are extrapolated from the interior points as done in [21].

5 Flow Conditions

In this paper, a high speed weakly ionized viscous flow in a supersonic wind tunnel with various imposed electromagnetic fields is considered. We consider two different stagnation pressures, i.e. one-third atmospheric pressure and one-fifth atmospheric pressure and several cases of magnetic fields, electric fields and electrical conductivities. The flow conditions that stay uniform are stagnation temperature, T_o=298K and Prandtl number, Pr=0.72.

In the current simulation the tunnel under consideration is approximately 0.208 m in length. The vertical width of the tunnel at its entrance is approximately 9.5 mm which increases to approximately 4 cm at tunnel exit. The tunnel width in spanwise direction is constant at approximately 2 cm. To increase the efficiency of three-dimensional calculations, inherent symmetry of the tunnel about a horizontal plane and a vertical plane is used. Thus, computational domain for simulation uses only a quarter of actual tunnel as flow in other parts of tunnel can be obtained using the symmetry about central planes in horizontal and vertical directions. The computational domain used for this study is presented in Fig. 1(a). The external fields are imposed between X=0.10m and X=0.154m (X=0 represents tunnel entrance). The spatially uniform electric field, which always points in the positive vertical direction, exists between those two points in the tunnel. The magnetic field acts in the spanwise direction between the same points.

6 MHD Effect on Steady Flow Solutions

The physical domain for three dimensional calculations is resolved using 80 stretch grids in the vertical direction, 26 stretch grids in the spanwise direction and 28 uniform grids in the streamwise direction. As a first step,

the cold flow was calculated with one third atmospheric stagnation pressure. Fig. 1(b) shows the Mach number contours along the length of the tunnel at several different planes perpendicular to the direction of flow. The contours clearly show fluid collecting at the centerline along the sidewalls. This can be attributed to a considerable cross flow in the wall normal direction, parallel to the sidewalls. Effects of sidewalls on the flow profile can be observed in Fig. 2(a) which shows lesser Mach numbers for the three dimensional calculations at the tunnel centerline as compared to those obtained for two dimensional calculations. This demonstrates that three-dimensional wall effect is significant for the flow which necessitates a three dimensional analysis. Having established the cold flow profile two separate cases of electric fields were considered while keeping stagnation pressure same i.e. one-third atmospheric pressure.

6.1 Case I: Effects of moderate electric fields on the cold flow

Figure 2(b) compares the Mach numbers at the centerline of the tunnel, for cold flow and three successively increasing electric fields of 1500V/m, 2000V/m and 2500V/m. It is clearly seen that the Mach numbers at the centerline drop as the electric fields are increased. Figure 3 compares the effects of moderate electric fields, i.e. 1500V/m, 2000V/m and 2500V/m for flow with $1/3^{rd}$ atmospheric stagnation pressure, on the boundary layer profile along the Y axis at different locations parallel to the sidewall. For the same cases Fig. 4 compares the boundary layer profile along the Z axis at different locations parallel to the test section bottom wall at the tunnel exit. From Figs. 3 and 4, it is seen that the flow retards with successively increasing electric fields. This is in accordance with the results obtained for two dimensional calculations [18] and demonstrates a direct consequence of Joule heating. Also, Mach number profile along Y axis show a significant drop in Mach number close to the center of the sidewall. This signifies a thick boundary layer on sidewall near the horizontal plane of symmetry.

6.2 Case II: Effects of electromagnetic fields on the cold flow, in both accelerating and retarding set ups

Figure 5 compares the Mach numbers for flow with electromagnetic field to those associated with cold flow. Magnetic fields of +1.5T and -1.5T has been applied on Joule heated flow with electric field of 30000 V/m. Figure 5(a) shows the Mach number contours in a Y-Z plane X=0.15m (0.15m downstream of the tunnel entrance for cold flow). Figure 5(b) shows the Mach number contours at the same location and in the same configuration for flow heated by an electric field of 30,000V/m. Clearly, an electric field of 30,000V/m retards the flow considerably. Also, the size of the cross flow bulge is seen to increase. However, the gradients in Mach number while moving away from the sidewall toward the centerline are seen to drop. Figure 5(c) and (d) show the Mach number contours in the Y-Z plane 0.15m downstream of the tunnel with a constant electric field of 30,000V/m but varying magnetic fields of +1.5T and -1.5T. For both the cases, a small area of circulation is observed near the centerline at the sidewall. However, with the magnetic field of -1.5T the region of flow circulation is seen to move away from the sidewall toward the centerline. Figures 6 and 7 compare the same parameters at X= 0.18m and X=0.208m (tunnel exit) respectively. Figures 5-7 clearly show that the size of the bulge progressively decreases downstream of the tunnel for the flows with electromagnetic fields. However, for the cold flow case, the secondary flow remains very strong and prominent. The Mach number is certainly lesser for flow with retarding magnetic field especially in the region close to centerline.

Figure 8 compares the streamwise vorticity in cold flow with flow altered by an electric field, and further with magnetic fields +1.5T and -1.5T. Figure 8(a) shows the streamwise vorticity contours in a Y-Z plane at X=0.15m for cold flow. Figure 8(b) shows the streamwise vorticity contours at the same location and in the same configuration for flow heated by an electric field of 30,000V/m. Clearly, the region of highest vorticity is seen to move toward the centerline away from the sidewall in the presence of an electric field. As the magnetic fields are turned on, it is clear from Figs. 8(c) and 8(d),that the gradients in streamwise vorticity drop as the distance normal to the sidewall increases. Figures 9 and 10 compare the streamwise vorticity at X=0.18m and X=0.208m (tunnel exit), respectively. It can be clearly seen that moving downstream of the zone of electromagnetic field imposition, magnitude of streamwise vorticity goes down considerably for the flow altered by electromagnetic fields while the streamwise vorticity for cold flow remains as is, without getting dissipated. Flows with a retarding magnetic field have considerably higher streamwise vorticity values as compared to those obtained for accelerating magnetic field in same situations.

Figure 11 shows the boundary layer profile along the Y axis at the exit of the tunnel, at different distances from the sidewall for cold flow, joule heated flow and flow further altered by additional magnetic fields. Figure 11(a) shows the boundary layer profiles at increasing distances from the wall for cold flow. Clearly, as we move away from the sidewall, the flow accelerates and the cross flow bulge also disappears. In Fig. 11(b) which shows the boundary layer profiles at the tunnel exit for flow altered by a constant electric field of 30,000V/m, the flow gets retarded which is a phenomena previously predicted by our two-dimensional calculations [18]. The cross flow bulge

is also seen to decrease when the electric field is turned on. Figure 11 (c) shows the comparison of boundary layers at different distances from the sidewall at the tunnel exit, with the electric field of 30,000V/m and the magnetic field of +1.5T. Once again, in keeping with the predictions of our two-dimensional calculations, the flow gets accelerated, though this effect is weak. Similarly with magnetic field of -1.5T the flow gets successively retarded at all locations parallel to the sidewall. Boundary layer profiles near sidewall show a bulge causing flow to slow down near the center of sidewall. This indicates presence of thick sidewall boundary layer near the centerline.

Figure 12 shows the boundary layer profiles along the Z axis at the exit of the tunnel, at different distances from the contoured wall for cold flow, joule heated flow and the flow further altered by additional magnetic fields. Figure 12(a) shows the boundary layer profiles at increasing distances from the wall for cold flow. Clearly, as we move towards the centerline, the flow accelerates. However, a sudden increase in boundary layer thickness is observed as we approach the centerline. That is attributed to the significant cross flow bulge in cold flow. Figure 12(b) shows the boundary layer profiles altered by an electric field of 30,000V/m. Clearly, it shows the gradients leading up to the cross flow bulge drop leading to a dissipation of the secondary flow seen in cold flow. Figure 12(c) and 12(d) show the profiles altered by an accelerating magnetic field and a decelerating magnetic field of + 1.5T and -1.5T respectively. Boundary layer on sidewall is particularly thick for all the cases shown in Fig. 12 which is a consequence of secondary flow present in that region.

To sum up, a strong secondary flow was observed in the tunnel even without application of electromagnetic fields. Flow is altered significantly by application of electromagnetic fields. For the cases considered in this study, retardation of flow by Joule heating dominates the mitigating effects of magnetic field. Just downstream of the zone of electromagnetic field imposition, a much stronger secondary flow is observed than that for cold flow at same location. However moving downstream towards the exit of tunnel, secondary flow reduces significantly for flows with electromagnetic fields applied. Flow obtained with electric field and a retarding magnetic field show very strong secondary flow as compared to other cases.

7 Calculations of flow fields assuming no Joule heating in the Energy Equation

The governing equation for conservation of energy (Eq. 4) does not consider any time lag between imposition of electric field and its effect on the flow through Joule heating. Following frozen flow analogy, another limit of this phenomenon may be the case when this time lag is so large that effect of Electric field is not felt as a source of heating in the flow. To explore this regime for flow field, calculations were performed by dropping the terms associated with Joule heating in the energy equation. Hence, instead of using Equation 4 as governing equation of energy flow following equation was used in conjunction with Eq. 2 and Eq. 3.

$$\frac{\partial e}{\partial t} + \nabla \cdot (e\mathbf{u}) = -\nabla \cdot (p\mathbf{u}) + \nabla \cdot (\mathbf{u} \cdot \overline{\overline{\tau}}) - \nabla \cdot \mathbf{q} \tag{14}$$

Under the assumption of "no Joule heating", electric field, if applied with magnetic field, contributes to Lorentz forces on the flow but does not produce any Joule heating. Considering equations used for this case it can be noted that applying only electric field will not have any effects on the cold flow in absence of magnetic field. This is in contrast with the results presented in section 6.2 where electric field was seen to be causing Joule heating of the flow which resulted in the considerable retardation of the flow. If a time lag exists between the imposition of electric field and Joule heating of the flow, we expect the actual results to be in between the two extremes presented in this section and section 6.2.

Calculations were performed for MHD flow under the assumption of "no Joule heating "with electric field of 30,000V/m and magnetic fields of +1.5T and -1.5T for stagnation pressures of 1/3rd atm i.e. conditions of section 6. Figure 13 compares Mach number and temperature at the centerline of tunnel for the flow obtained without considering Joule heating effect to those obtained for flow heated by electromagnetic field. As we study Mach number variation along center line of tunnel (Fig. 13(a)), it is readily observed that Mach number is considerably higher for the curves obtained by neglecting Joule heating effects than those obtained for flow retarded by Joule heating. The region of imposition of electromagnetic field is approximately between X=0.10m and X=0.154m. Mach number at centerline, calculated without Joule heating effects for accelerating electromagnetic field of E=30000 V/m and B=+1.5T, clearly increases as compared to the cold flow and in the region of imposition of field this increase is monotonous. The outcome is opposite for retarding electromagnetic field. It can be seen from Fig. 13(a) the dependence of Mach number on magnetic field is much complex if Joule heating effects are considered. As compared to cold flow, Mach number at centerline calculated without Joule heating effects, is seen to be increasing

by a value of approximately 6.5% with respect to cold flow, at the exit of test section for accelerating magnetic field while it decreases by approximately 6.2% at same location for retarding electromagnetic field. Figure 13(b) shows temperature variation along the centerline of tunnel. It can be seen that Joule heating causes a considerable rise of temperature which results in decrease in Mach number for the corresponding flow while the temperature in flow is almost constant for the cases calculated under assumption of no Joule heating.

For a better presentation of spatial variation of Mach number in the flow, Figs. 14,15 and 16 compare contours of Mach number for MHD flow with those obtained for cold flow at X=0.10m, X=0.154m and X=0.208m, respectively. X=0.10 m represents location where region of imposition of electromagnetic field begins. Since flow has not encountered electromagnetic before X=0.10, Mach number isocontours at this location are very similar (Fig. 14) for cold flow as well as flow with MHD forces. However, small decrease shown by the flow with opposing electromagnetic field can be explained by the viscous effects causing downstream-flow to slow down as upstream flow is retarded. After the flow has passed through electromagnetic field, effects of MHD forces on the flow are more prominent as presented in Fig. 15. Further downstream of the point where imposition of electromagnetic field ends, changes in Mach numbers are small for all the cases. Resulting isocontours of Mach number at the exit of tunnel are shown in Fig. 16.

Similar to cold flow, Mach number contours for MHD flow without Joule heating also show a bulge near the central height of sidewall which signifies a region of secondary flow. To compare the extent of secondary flow near the side wall streamwise vorticity has been plotted in Figs. 17,18 and 19 corresponding to locations X=0.10m, X=0.154m and X=0.208m respectively. Before application of electromagnetic field streamwise vorticity profile are nearly same for cold flow as well as flow with MHD forces (Fig. 17). However after passing through electromagnetic field, flow calculated with retarding magnetic field shows higher values of streamwise vorticity as compared to those obtained for cold flow. On the other hand, for the accelerating electromagnetic field streamwise vorticity has lesser values in general to those obtained from cold flow calculations. These observations go along well with the Mach number contours as bulge near sidewall gets more prominent as opposing electromagnetic field is applied. Comparing Figs. 18 and 19, drops in streamwise vorticity values are observed while going downstream of the zone of imposition of electromagnetic fields, for cold flow as well as flow calculated with electromagnetic fields under assumption of no Joule heating. However, these drops are not as drastic as obtained for Joule heated flow with same electromagnetic fields in section 6.2. Figure 20 and 21 present comparisons of boundary layer profiles in vertical and spanwise direction at several locations. Boundary layer profile looks almost same with or without MHD forces if Joule heating is not considered. For all the cases, boundary layer in spanwise direction is very thick near central height (Fig. 21) which is in accordance with the observations made for streamwise vorticity contours and Mach number contours.

Overall, considering the results obtained for flows calculated with the assumption of no Joule heating, it seems that magnetic field should be used in the accelerating direction to have an accelerated flow with a weaker secondary flow.

8 Effect of changing pressure on MHD flow

Flows with lower Reynolds number are expected to have a thicker boundary layer which should stabilize the flow. This scenario was explored by performing calculations for an inlet flow with stagnation pressure of $1/5^{th}$ atmospheric pressure. It should be noted that the results presented in section 6 and 7 were obtained for higher stagnation pressure of $1/3^{rd}$ atmospheric pressure.

8.1 Case I. Effects of changing stagnation pressure on cold flow

Figure 22 compares Mach number variation profile in Y direction, at the exit of the tunnel for cold flow with stagnation pressures of $1/3^{rd}$ atm and $1/5^{th}$ atm at various distances from the sidewall. Stagnation temperature is kept same for both cases. Figure 22(d) shows that Mach number near centerline is almost same for both the flows as expected for inviscid adiabatic flows with same stagnation temperatures. However, moving away from centerline of tunnel Mach number reduces faster in case of lower stagnation pressure as can be observed from Figs 22(a), 22(b) and 22(c). Mach numbers are particularly low near the center line of tunnel. This signifies the fact that boundary layer developed on side wall is thicker for lower stagnation pressure case especially near mid-height of the sidewall. This is expected as viscous effects are stronger for this lower Reynolds number flow. Figure 23 compares boundary layers in spanwise direction in the tunnel at different heights, at the exit of tunnel (X=0.208m). It can again be inferred that moving away from centerline of tunnel flow slows down more sharply in the case of lower stagnation pressure and boundary layers are thicker for flow with lower stagnation pressure. Figure 23(d) shows that boundary

layer is particularly thick near the centerline of sidewall for lower Reynolds number flow which corresponds to stronger secondary flow than that obtained for flow with higher stagnation pressure in section 6.1.

Figure 24 compares Mach number contours in Y-Z plane at X=0.15m for the flows with inlet stagnation pressures of 1/3rd atm and 1/5th atm respectively .Mach number contours have a bulge near the center height of the tunnel (for both the flows). This means that flow is more retarded by the sidewall near the centre of each sidewall, which gives rise to secondary cross flow in the tunnel. The bulge in the Mach number contour is much prominent in the case of lower stagnation pressure leading to stronger cross flow. This is confirmed by Fig. 25 which shows contours of streamwise vorticity Y-Z plane at same location i.e. (X=0.15m).Larger vorticity contours (indicating stronger cross flow) are observed for flow with lower stagnation pressure. Also for lower stagnation pressure case the point of maximum vorticity seems to be slightly shifted away from horizontal plane of symmetry. As can be seen from Figs. 26 and 28, moving along the flow direction, the high Mach number isocontours shrink more rapidly in the case of lower stagnation pressure and the bulge becomes more pronounced although Mach number at center line remains almost same in both the cases. Streamwise vorticity plots (Figs. 27 and 29) further confirm that stronger secondary flow is obtained for flow with lower Reynolds number. Hence contrary to the expectation, stronger viscous effects do not stabilize the secondary flow.

8.2 Case II: Effects of electromagnetic fields on the cold flow

For stagnation pressure of 1/5th atm, the energy imparted by Joule heating is expected to be much higher than the energy of the fluid entering into the tunnel. However, if we neglect the Joule heating effects, independent effects of Lorentz forces can be noted on the flow. The results for calculations under the assumption of "no Joule heating" show a direct dependence on the direction of magnetic field as can be seen from Fig. 30. When flow passes through an accelerating magnetic field, Mach number increases by up to 13.8% (at the end of imposition of electromagnetic field centerline of tunnel) with respect to cold flow. While a decrease of approximately 10% is observed at the same location if the direction of magnetic field is reversed. Such direct dependence of Mach number on direction of magnetic field is expected under the simplifying assumption of no Joule heating. Comparing these results with those obtained for inlet flow at stagnation pressure of 1/3rd atm, it is observed that in absence of Joule heating, effect of Lorentz forces is more pronounced in the case of lower stagnation pressure which causes a greater increase or decrease in Mach number of the flow with lower stagnation pressure while electromagnetic fields are kept same. This is further confirmed by observation of Mach number contours at the exit of test section (Fig. 31) in the plane perpendicular to streamwise direction. Also, the bulge in Mach number contours is observed which is more prominent for the flow with retarding magnetic field. This trend is similar to that observed for the case of higher Reynolds number flow (section 7). Figure 32 confirms that under the assumption of no Joule heating an accelerating magnetic field will be helpful for reducing secondary flow in the test section of tunnel.

The solutions obtained with the assumption of no Joule heating, for both inlet stagnation pressure conditions considered in this study; clearly recommend use of accelerating magnetic fields to obtain accelerated flow with a weaker secondary flow. For Joule heated flow, high secondary flow is produced for flow with retarding magnetic fields. Since actual flows are expected to be in between the solutions obtained by with and without considering Joule heating effects, we can say that in comparison to a retarding field, an accelerating magnetic field is more likely to reduce secondary flow in the tunnel.

9 Conclusion

Weakly ionized supersonic flow in a tunnel in presence of a number of imposed electromagnetic fields was studied by three dimensional numerical simulation of Navier-Stokes equation. Strong secondary flow was observed in the tunnel even in absence of electromagnetic forces. The main focus was on study of secondary flow in steady state solutions at test section of the high speed tunnel with variation of MHD forces and stagnation pressure.

The steady flow results show that all imposed electromagnetic fields cause significant Joule heating of flow altering the boundary layer profile significantly. For high electric fields in isolation of the magnetic field, localized heating in the vicinity of the electric field is observed causing a significant retardation of mean flow. The magnetic fields applied in the study have very small effect on the flow in comparison to the alternations made on the flow due to Joule heating. In the zone where electromagnetic fields are applied, secondary flow becomes even stronger than that observed in the cold flow but it reduces significantly moving to exit of tunnel downstream of the field of imposition of electromagnetic field. A retarding magnetic field applied in conjunction with electric field was seen to cause much stronger secondary flow as compared to the accelerating magnetic field.

In actual flow there might be a time lag between imposition of electric field and Joule heating of the flow and if this is significant we can neglect the Joule heating terms in energy equation. Solutions obtained with this assumption

represent another extreme which actual flow can be expected to follow. Steady flow solution under the assumption of no Joule heating show a direct dependence (acceleration or retardation of flow) on magnitude and direction of magnetic flow applied. However alternations to base flow are not as strong as those obtained for flow with Joule heating. An increase in strength of secondary flow is observed for retarding magnetic field.

For lower Reynolds number flow, viscous effects are stronger which are expected to stabilize the flow. Contrary to expectation, thicker sidewall boundary layer causes a stronger secondary flow. Simulations done by neglecting Joule heating effects show that effects of electromagnetic field are more prominent for the lower Reynolds number flow.

For almost all of the studies done in the paper, it was observed that accelerating magnetic field applied with electric field causes weaker secondary flow as compared to retarding magnetic field.

Acknowledgments

This research was supported by Innovative Scientific Solutions Inc., Dayton, Ohio and the Air Vehicles Directorate of Air Force Office of Scientific Research, under an SBIR Phase II contract. The authors would like to thank Drs. J W Rich, I Adamovich of the Ohio State University and Dr. R L Kimmel of the Air Force Research Laboratory, Dayton, Ohio for their valuable suggestions during the course of this work.

References

[1] Shang, J.S., "An outlook of CEM multidisciplinary applications", AIAA paper 99-0336, 1999.

[2] Canupp, P. W., "The influence of magnetic fields for shock waves and hypersonic flows", AIAA paper 2000-2260, 2000.

[3] Damevin, H., Dietiker, J., and Hoffmann, K. A., "Hypersonic flow computations with magnetic field", AIAA paper 2000-0451, 2000.

[4] Agarwal, R. K., and Augustinus, J., "Numerical simulation of compressible viscous MHD flows for reducing supersonic drag of blunt bodies", AIAA paper 99-0601,1999.

[5] Hoffmann, K. A., Damevin, H., and Dietiker, J., "Numerical simulation of hypersonic magnetohydrodynamic flows", AIAA paper 2000-2259, 2000.

[6] Poggie, J., and Gaitonde, D. V., "Magnetic control of hypersonic blunt body flow", AIAA paper 2000-0452, 2000.

[7] Gaitonde, D. V., "Development of solver for 3-D nonideal magnetogasdynamics", AIAA paper 99-3601, 1999.

[8] Shang, J. S., Canupp, P. W. and Gaitonde, D. V., "Computational magneto-aerodynamic hypersonics", AIAA paper 99-4903, 1999

[9] McMullan, R. J., Lindsey, M. F. and Adamovich, I. V., "Experimental validation of 3-D magnetogasdynamic compressible Navier-Stokes solver", AIAA paper 2004-2269, 2004.

[10] Updike, G. A., Shang, J. S. and Gaitonde, D. V., "Hypersonic separated flow control using magneto-aerodynamic interaction", AIAA paper 2005-164, 2005.

[11] Kimmel, R. L., Hayes, J. R., Menart, J. A. and Shang, J., "Application of plasma discharge arrays to high-speed flow control" AIAA paper 2005-0946, 2005.

[12] Poggie, J., "Computational studies of high-speed flow control with weakly ionized plasma", AIAA paper 2005-0784, 2005.

[13] Gaitonde, D. V., "Simulation of local and global high-speed flow control with magnetic fields", AIAA paper 2005-0560, 2005.

[14] Palm, P., Meyer, R., Plönjes, E., Bezant, A., Adamovich, I. V., Rich, J. W. and Gogineni, S., "MHD effect on a supersonic weakly ionized flow", AIAA-2002-2246, 2002.

[15] Meyer, R., Chintala, N., Bystricky, B., Hicks, A., Cundy, M., Lempert, W. R. and Adamovich, I. V., "Lorentz force effect on a supersonic ionized boundary layer", AIAA paper 2004-0510, 42nd Aerospace Sciences Meeting and Exhibit, January 2004, Reno, NV.

[16] Meyer, R., McEldowney, B., Chintala, N., Palm, P. and Adamovich, I.V., "Experimental studies of plasma assisted ignition and MHD Supersonic Flow Control", AIAA paper 2003-0873, presented at 41st Aerospace Sciences Meeting and Exhibit, January 2003, Reno, NV.

[17] McEldowney, B., Meyer, R., Chintala, N. and Adamovich, I. V., "Measurements of electrical parameters of a supersonic nonequilibrium MHD channel", AIAA Paper 2003-4279, presented at 34th Plasmadynamics and Lasers Conference, Orlando, FL, 23-26 June 2003.

[18] Singh, V., Zhong, X. and Gogineni, S., "Numerical simulation of supersonic boundary layer stability with applied electromagnetic field in a weakly ionized flow", AIAA paper 2004-2724, 2004.

[19] Augustinus, J., Hoffmann, K. A. and Harada, S., "Numerical solutions of ideal MHD equations for a symmetric blunt body at hypersonic speeds", AIAA Paper 98-0850, 1999.

[20] Gaitonde, D. V., "Development of a solver for 3-D non-ideal magnetogasdynamics", AIAA paper 99-3610, 1999.

[21] Zhong, X., "High-order finite-difference schemes for numerical simulation of hypersonic boundary-layer transition", Journal of Computational Physics, Vol. 144, August 1998, pp. 662-709.

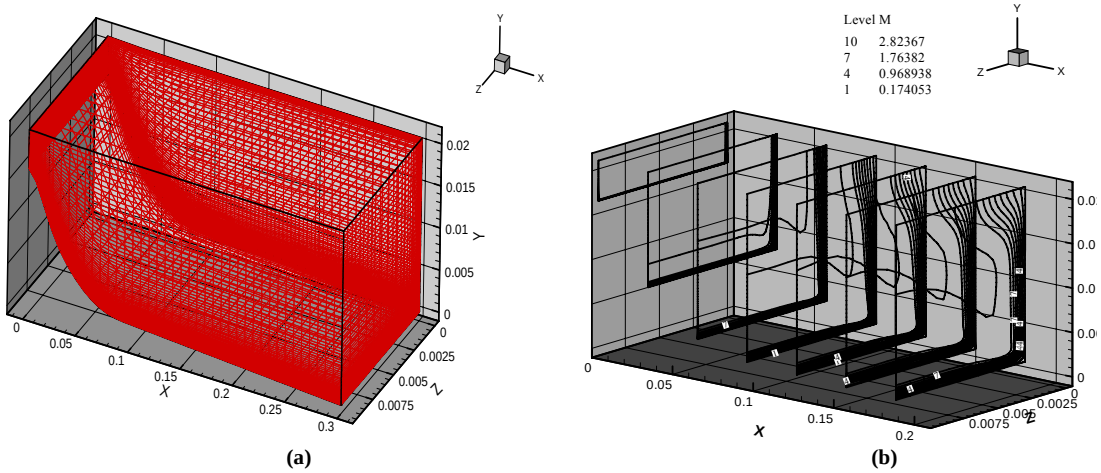

Figure 1.For three dimensional computations (a) grid used for simulations on the MHD supersonic tunnel(b) Mach contours for cold flow at different X locations at stagnation pressure of 1/3rd atm.

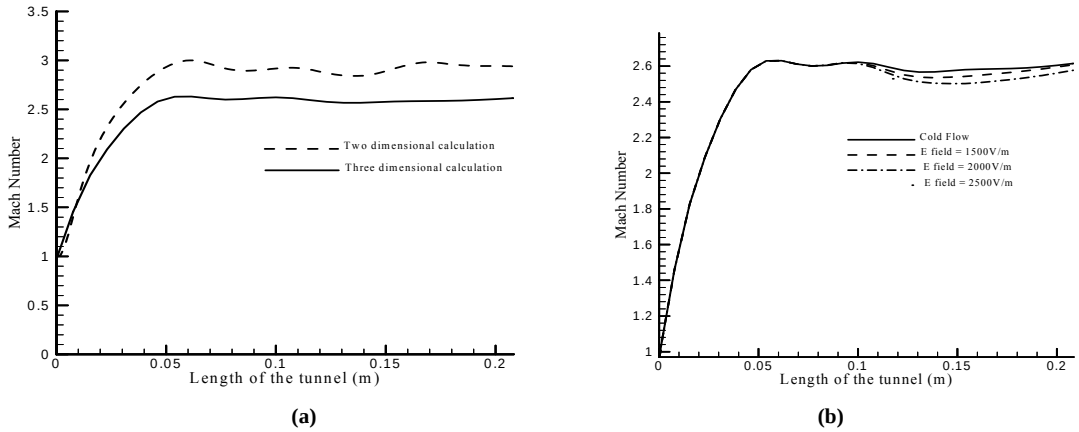

Figure2. *The Mach number comparison along tunnel centerline for (a) two dimensional and three dimensional calculations (b)for increasing values of electric field with electric conductivity of 0.5 mho/m.(stagnation pressure=1/3rd atm).*

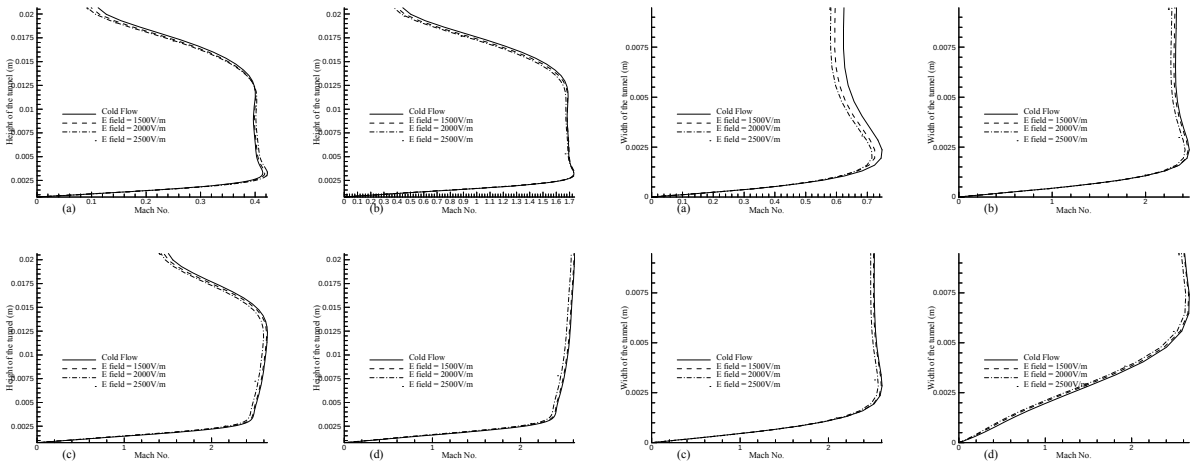

Figure 3. *Boundary layer profiles along the Y axis at the tunnel exit, at increasing distances from the sidewall for cold flow and electric fields of 1500V/m, 2000V/m and 2500V/m, at (a) z = 0.00018m, (b) z = 0.00084m, (c) z = 0.00284m and (d) z = 0.01m (σ=0.5mho/m, P_0=1/3rd atm).*

Figure 4. *Boundary layer profiles along the Z axis at the tunnel exit, at increasing distances from the bottom wall for cold flow and electric fields of 1500V/m, 2000V/m and 2500V/m, at (a) y = 0.00123m, (b) y = 0.0028m, (c) y = 0.0076m and (d) y = 0.021m.(σ=0.5mho/m, P_0=1/3rd atm)*

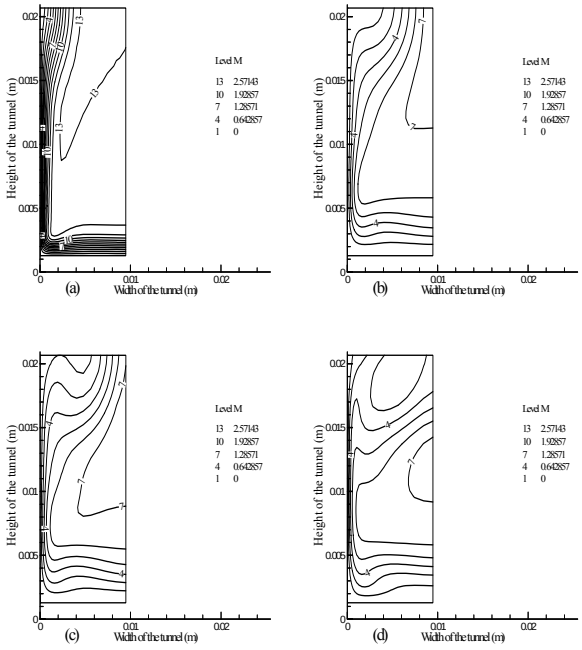

Figure 5. *A comparison of Mach numbers in a Y-Z plane at X = 0.15m for (a) Cold Flow, (b) Flow heated with an electric field of 30,000V/m,(c) Flow heated with 30,000V/m and a magnetic field of +1.5T and (d) Flow heated with 30,000V/m and a magnetic field of -1.5T.(electrical conductivity = 0.1mho/m,stagnation pressure=1/3rd atm).*

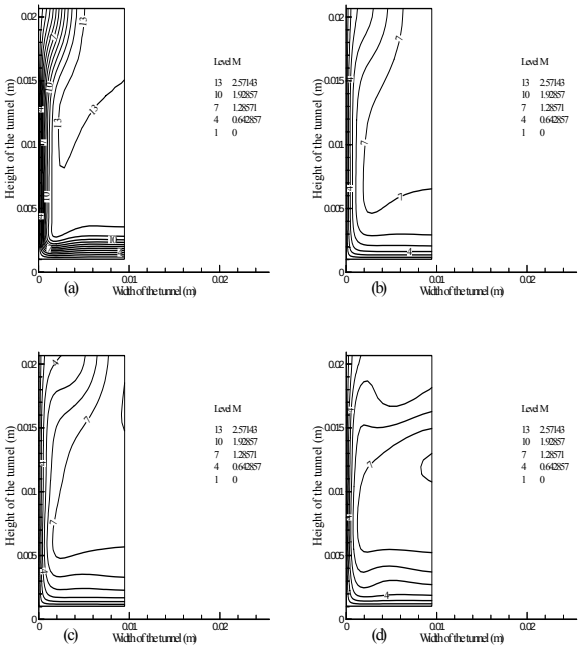

Figure 6. *A comparison of Mach numbers in a Y-Z plane at X = 0.180m for (a) Cold Flow, (b) Flow heated with an electric field of 30,000V/m,(c) Flow heated with 30,000V/m and a magnetic field of +1.5T and (d) Flow heated with 30,000V/m and a magnetic field of -1.5T. (electrical conductivity = 0.1mho/m,stagnation pressure=1/3rd atm).*

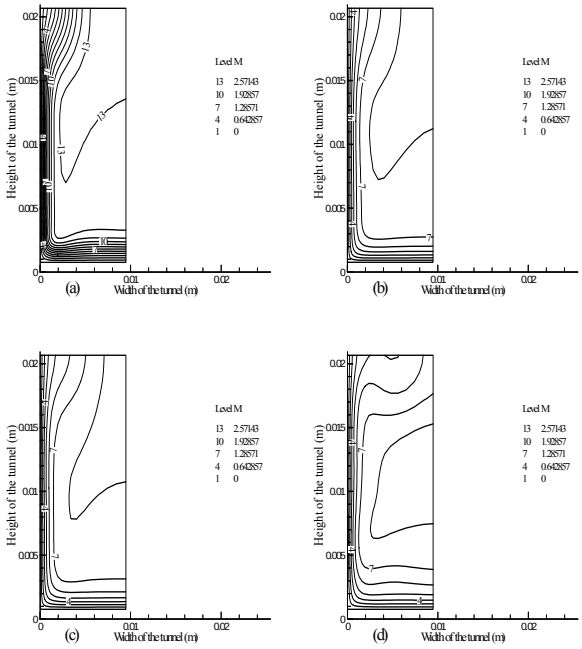

Figure 7. *A comparison of Mach numbers in a Y-Z plane at X = 0.208m for (a) Cold Flow, (b) Flow heated with an electric field of 30,000V/m,(c) Flow heated with 30,000V/m and a magnetic field of +1.5T and (d) Flow heated with 30,000V/m and a magnetic field of -1.5T. (electrical conductivity = 0.1mho/m,stagnation pressure=1/3rd atm)*

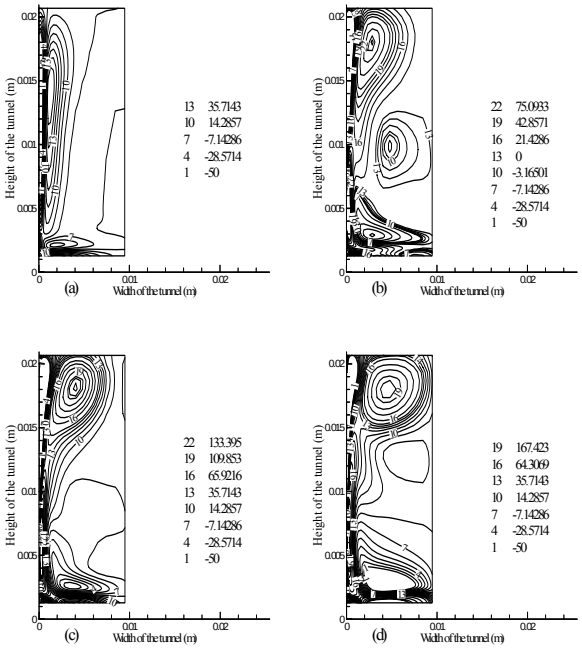

Figure 8. *A comparison of streamwise vorticity in a Y-Z plane at X = 0.15m for (a) Cold Flow, (b) Flow heated with an electric field of 30,000V/m,(c) Flow heated with 30,000V/m and a magnetic field of +1.5T and (d) Flow heated with 30,000V/m and a magnetic field of -1.5T. (σ= 0.1mho/m,stagnation pressure=1/3rd atm).*

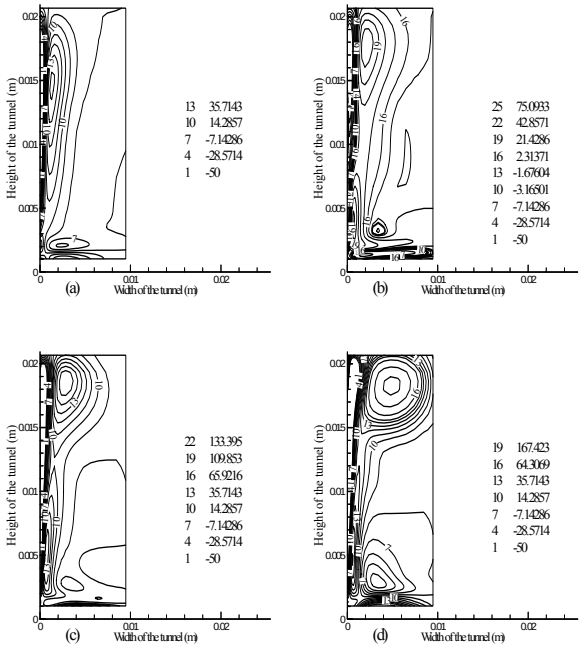

Figure 9. *A comparison of streamwise vorticity in a Y-Z plane at X = 0.180m for (a) Cold Flow, (b) Flow heated with an electric field of 30,000V/m,(c) Flow heated with 30,000V/m and a magnetic field of +1.5T and (d) Flow heated with 30,000V/m and a magnetic field of -1.5T (σ=0.1mho/m,stagnation pressure=1/3rd atm).*

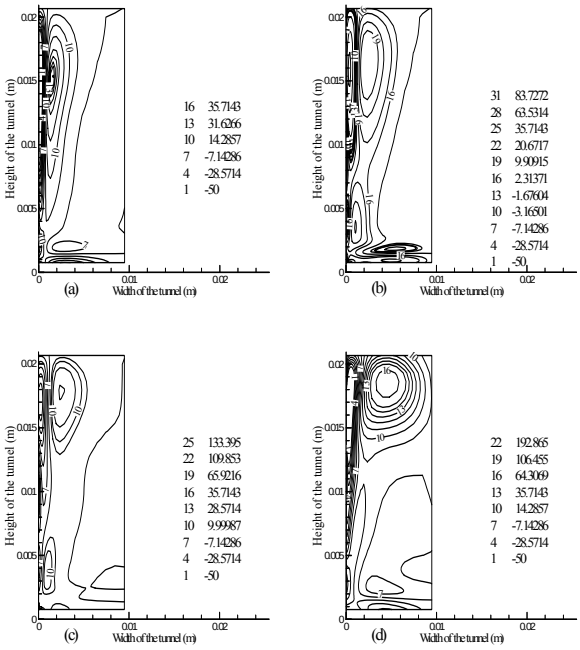

Figure 10. *A comparison of streamwise vorticity in a Y-Z plane at X = 0.208m for (a) Cold Flow, (b) Flow heated with an electric field of 30,000V/m,(c) Flow heated with 30,000V/m and a magnetic field of +1.5T and (d) Flow heated with 30,000V/m and a magnetic field of -1.5T (σ=0.1mho/m,stagnation pressure=1/3rd atm).*

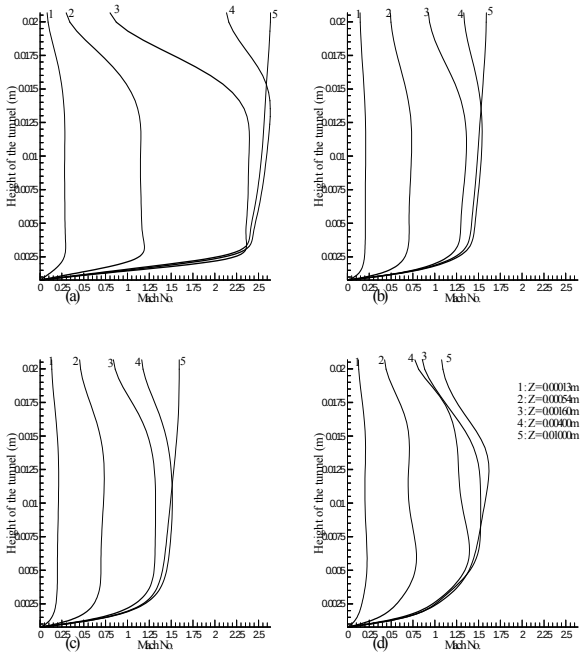

Figure 11. *Boundary layer profiles along the Y axis at the tunnel exit, at increasing distances from the sidewall for (a) Cold Flow,(b) Flow heated with E_y=30,000V/m,(c) Flow heated with E_y=30,000V/m and B_z=+1.5T and (d) Flow heated with E_y=30,000V/m and B_z= -1.5T. (σ= 0.1mho/m,stagnation pressure=1/3rd atm).*

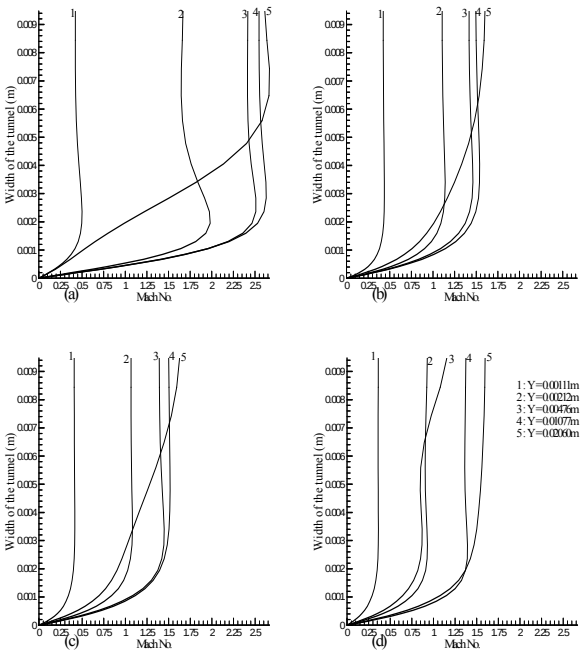

Figure 12. *Boundary layer profiles along the Z axis at the tunnel exit, at increasing distances from the bottom wall for (a) Cold Flow,(b) Flow heated with E_y=30,000V/m,(c) Flow heated with E_y=30,000V/m and B_z= +1.5T and (d) Flow heated with E_y=30,000V/m and B_z= -1.5T. (σ= 0.1mho/m,stagnation pressure=1/3rd atm).*

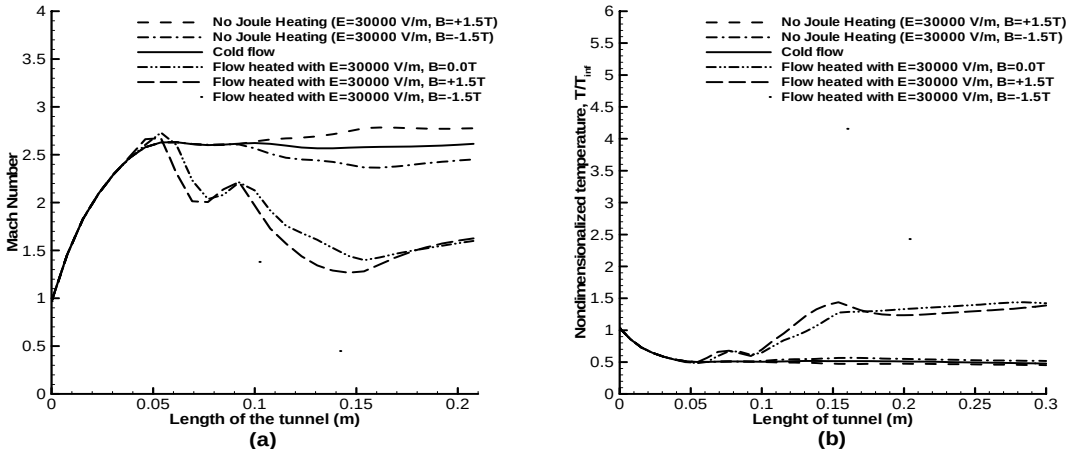

Figure 13. *Comparisons of (a) Mach number variation (b) Temperature variation along centerline of tunnel for flow computed by disregarding Joule heating to those where flow is heated by electric field.(σ= 0.1mho/m,stagnation pressure=1/3rd atm)*

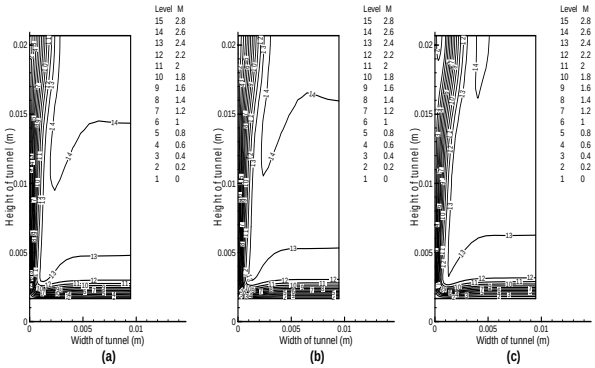

Figure 14. *Comparison of Mach number isocontours in Y-Z plane at X=0.1m (start of imposition of electromagnetic field) for (a) Flow computed with no Joule Heating for accelerating magnetic field (E=30000 V/m and B=+1.5T) (b) Cold flow. (c) Flow computed with no Joule Heating for decelerating magnetic field (E=30000 V/m and B=-1.5T). (σ= 0.1mho/m,stagnation pressure=1/3rd atm)*

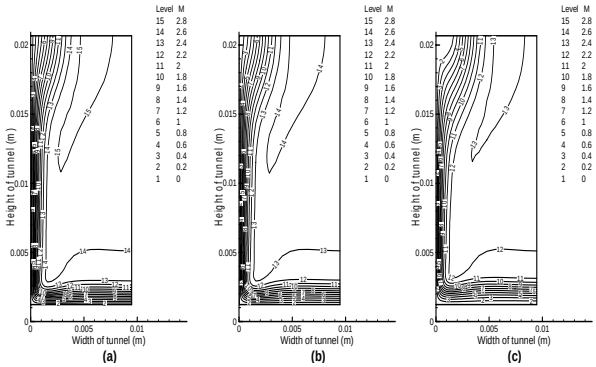

Figure 15. *Comparison of Mach number isocontours in Y-Z plane at X=0.154m (end of imposition of electromagnetic field) for (a) Flow computed with no Joule Heating for accelerating magnetic field (E=30000 V/m and B=+1.5T) (b) Cold flow. (c) Flow computed with no Joule Heating for decelerating magnetic field (E=30000 V/m and B=-1.5T). (σ= 0.1mho/m,stagnation pressure=1/3rd atm)*

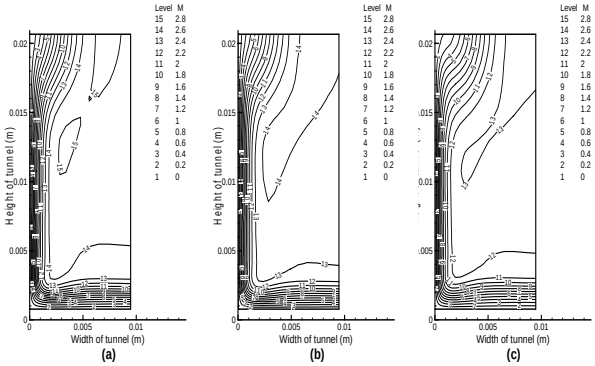

Figure 16. *Comparison of Mach number isocontours in Y-Z plane at X=0.208m (exit of test section) for (a) Flow computed with no Joule Heating for accelerating magnetic field (E=30000 V/m and B=+1.5T) (b) Cold flow. (c) Flow computed with no Joule Heating for decelerating magnetic field (E=30000 V/m and B=-1.5T). (σ= 0.1mho/m, stagnation pressure=1/3rd atm)*

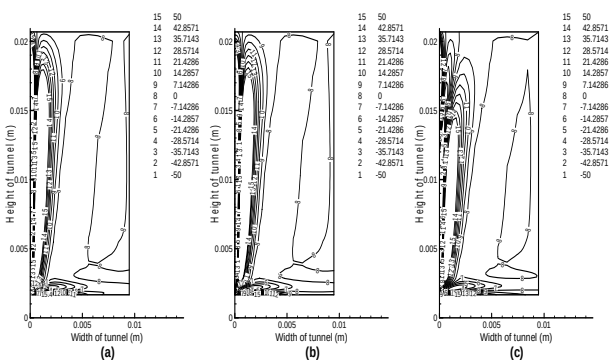

Figure 17. *Comparison of isocontours of streamwise vorticity in Y-Z plane at X=0.10m (start of imposition of electromagnetic field)for (a) Flow computed with no Joule Heating for accelerating magnetic field (E=30000 V/m and B=+1.5T) (b) Cold flow. (c) Flow computed with no Joule Heating for decelerating magnetic field (E=30000 V/m and B=-1.5T). (σ= 0.1mho/m, stagnation pressure=1/3rd atm).*

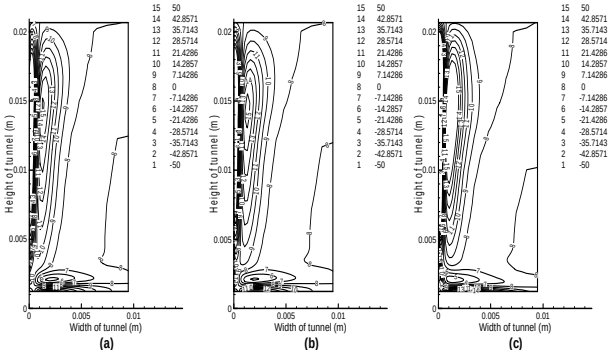

Figure 18. *Comparison of isocontours of streamwise vorticity in Y-Z plane at X=0.154m (end of imposition of electromagnetic field) for (a) Flow computed with no Joule Heating for accelerating magnetic field (E=30000 V/m and B=+1.5T) (b) Cold flow. (c) Flow computed with no Joule Heating for decelerating magnetic field (E=30000 V/m and B=-1.5T). (σ= 0.1mho/m, stagnation pressure=1/3rd atm).*

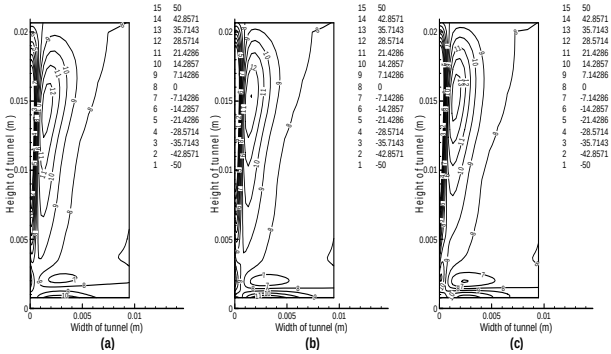

Figure 19. *Comparison of isocontours of streamwise vorticity in Y-Z plane at X=0.208m (exit of test section) for (a) Flow computed with no Joule Heating for accelerating magnetic field (E=30000 V/m and B=+1.5T) (b) Cold flow. (c) Flow computed with no Joule Heating for decelerating magnetic field (E=30000 V/m and B=-1.5T). Stagnation Pressure=1/3rd atm, Electric conductivity = 0.10 mho/m.*

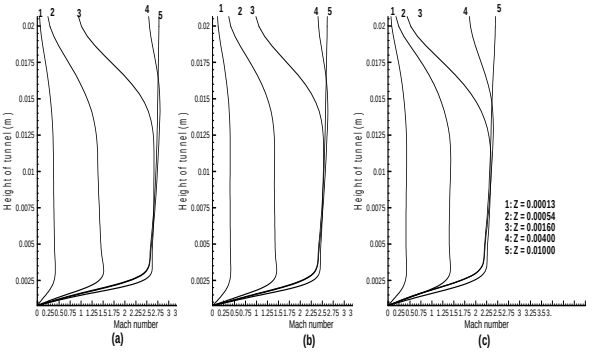

Figure 20. *Boundary layer profiles along the Y axis at the tunnel exit, at increasing distances from the sidewall for (a) Flow computed with no Joule Heating for accelerating magnetic field (E=30000 V/m and B=+1.5T) (b) Cold flow. (c) Flow computed with no Joule Heating for decelerating magnetic field (E=30000 V/m and B=-1.5T).(Stagnation Pressure=1/3rd atm, Electric conductivity = 0.10 mho/m).*

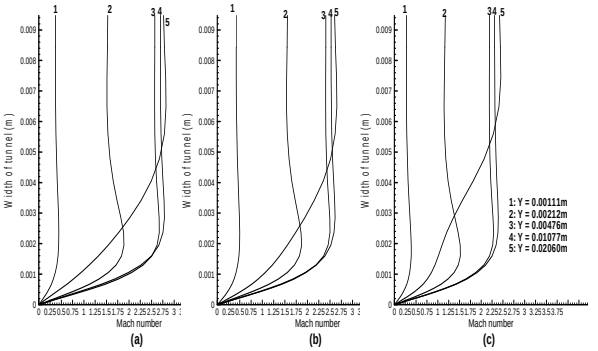

Figure 21. *Boundary layer profiles along the Z axis at the tunnel exit, at increasing distances from bottom wall for (a) Flow computed with no Joule Heating for accelerating magnetic field (E=30000 V/m and B=+1.5T) (b) Cold flow. (c) Flow computed with no Joule Heating for decelerating magnetic field (E=30000 V/m and B=-1.5T).(Stagnation Pressure=1/3rd atm, Electric conductivity = 0.10 mho/m).*

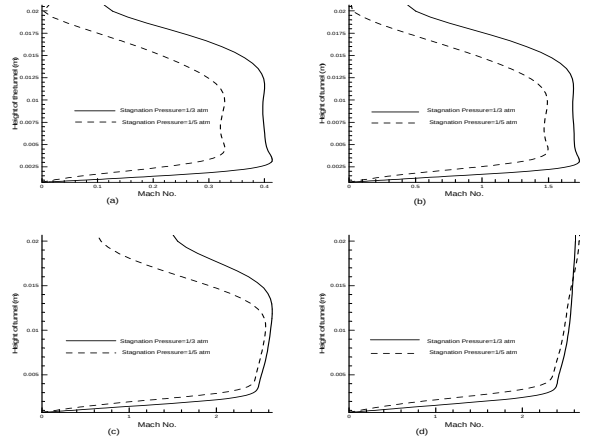

Figure 22. *Boundary layer profile in Y direction, at tunnel exit for cold flow with stagnation pressures of 1/3rd atm (solid) and 1/5th atm (dashed) at (a) z = 0.00018m, (b) z = 0.00084m, (c) z = 0.00284m and (d) z = 0.01m*

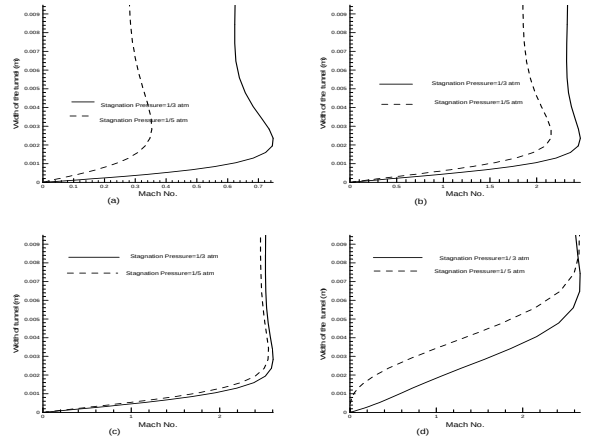

Figure 23. *Boundary layer profile in Z direction, at tunnel exit for cold flow with stagnation pressures of 1/3rd atm (solid) and 1/5th atm(dashed) at (a) y = 0.00123m, (b) y = 0.0028m, (c) y = 0.0076m and (d) y = 0.021m.*

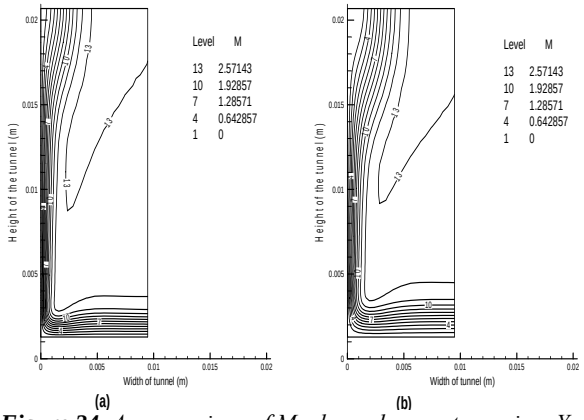

Figure 24. *A comparison of Mach number contours in a Y-Z plane at X = 0.15m for cold flow with stagnation pressure of (a) 1/3rd atm (b) 1/5th atm.*

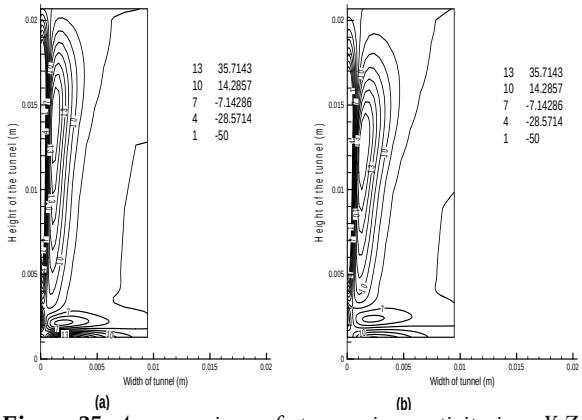

Figure 25. *A comparison of streamwise vorticity in a Y-Z plane at X = 0.15m for cold flow with stagnation pressure of (a) 1/3rd atm (b) 1/5thatm.*

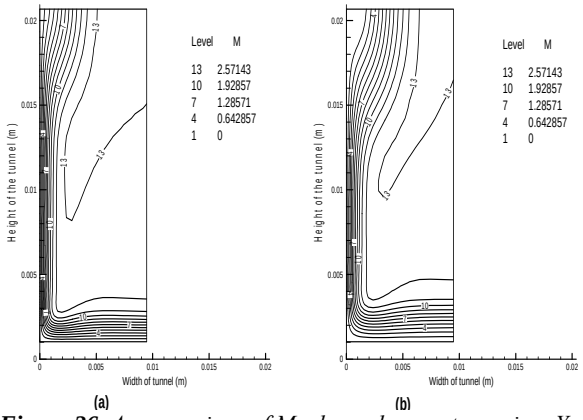

Figure 26. *A comparison of Mach number contours in a Y-Z plane at X = 0.180m for cold flow with stagnation pressure of (a) 1/3rd atm (b) 1/5th atm..*

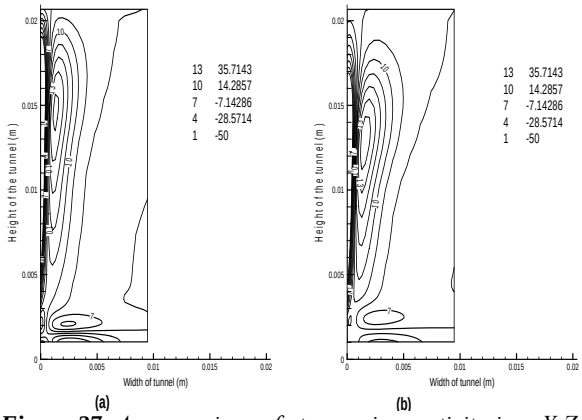

Figure 27. *A comparison of streamwise vorticity in a Y-Z plane at X = 0.180m for cold flow with stagnation pressure of (a) 1/3rd atm (b) 1/5thatm.*

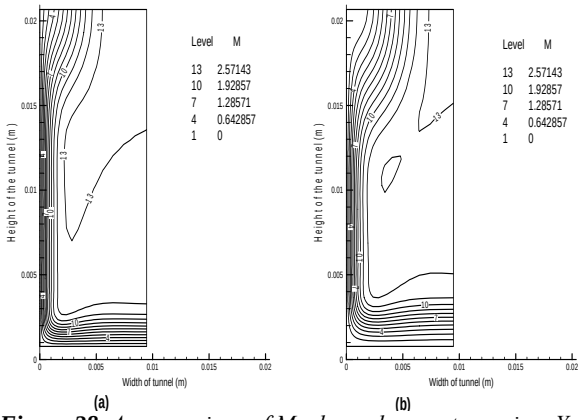

Figure 28. *A comparison of Mach number contours in a Y-Z plane at X = 0.208m for cold flow with stagnation pressure of (a) 1/3rd atm (b) 1/5thatm.*

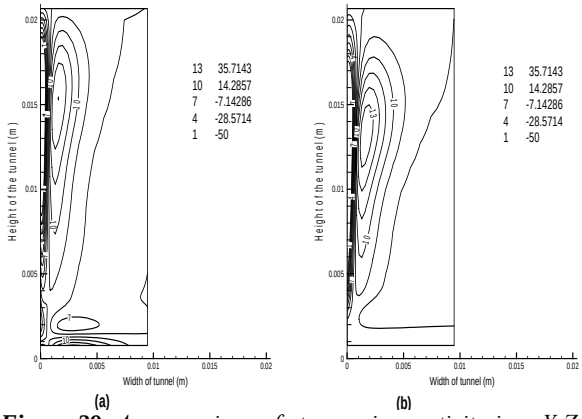

Figure 29. *A comparison of streamwise vorticity in a Y-Z plane at X = 0.208m for cold flow with stagnation pressure of (a) 1/3rd atm (b) 1/5thatm.*

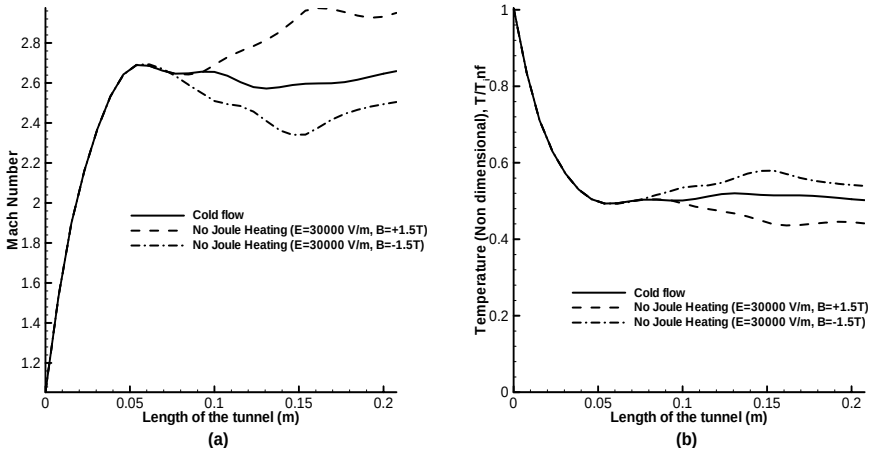

Figure 30. *(a)Mach number and (b) Temperature variation along centerline of tunnel for flow at lower stagnation pressure of 1/5th atm cold flow and flow with accelerating and decelerating electromagnetic fields assuming no Joule heating of flow. (electrical conductivity = 0.1mho/m)*

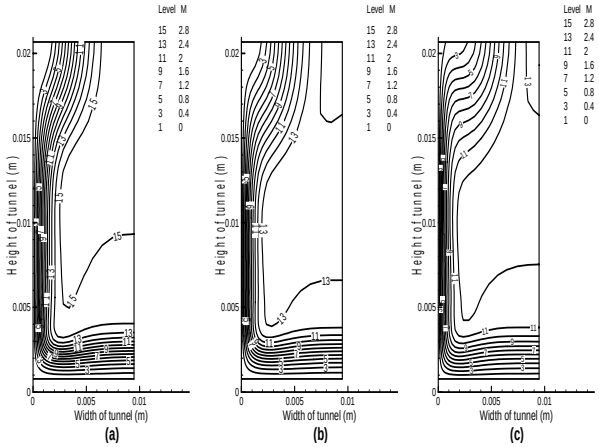

Figure 31. *Comparison of Mach number contours at tunnel exit, obtained under assumption of no Joule heating for stagnation pressure of 1/5th atm for (a) Flow with E=30000 V/m, B=+1.5T (b) Cold flow (c) Flow with E=30000 V/m, B=-1.5T*

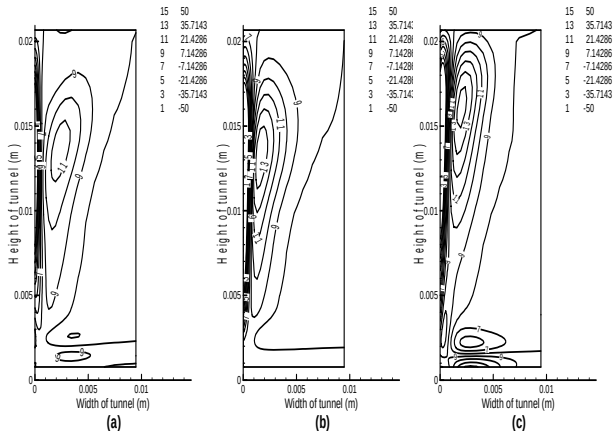

Figure 32. *Comparison of contours of streamwise vorticity at tunnel exit, obtained under assumption of no Joule heating for stagnation pressure of 1/5th atm for (a) Flow with E=30000 V/m, B=+1.5T (b) Cold flow (c) Flow with E=30000 V/m, B=-1.5T*